3D Reconstruction of Coronary Artery Stents From Optical Coherence Tomography: Experimental Validation and Clinical Feasibility

Wei Wu
Cardiovasclar Biology and Biomechanics Laboratory, Cardiovascular Division, University of Nebraska Medical Center, Omaha, Nebraska

Khan Behram A.
Cardiovasclar Biology and Biomechanics Laboratory, Cardiovascular Division, University of Nebraska Medical Center, Omaha, Nebraska

Mohammadali Sharzehee
Cardiovasclar Biology and Biomechanics Laboratory, Cardiovascular Division, University of Nebraska Medical Center, Omaha, Nebraska

Shijia Zhao
Cardiovasclar Biology and Biomechanics Laboratory, Cardiovascular Division, University of Nebraska Medical Center, Omaha, Nebraska

Saurabhi Samant
Cardiovasclar Biology and Biomechanics Laboratory, Cardiovascular Division, University of Nebraska Medical Center, Omaha, Nebraska

Yusuke Watanabe
Department of Cardiology, Teikyo University Hospital, Tokyo

Yoshinobu Murasato
Department of Cardiology, National Hospital Organization Kyushu Medical Center, Fukuoka

Timothy Mickley
Boston Scientific Inc, Hamel, Minnesota

Andrew Bicek
Boston Scientific Inc, Hamel, Minnesota

Richard Bliss
Medtronic Inc, San Francisco, California

Francesco Burzotta
Department of Cardiovascular Sciences, Fondazione Policlinico Universitario A. Gemelli IRCCS Università Cattolica del Sacro Cuore, Rome

Habib Samady
School of Medicine, Emory University, Atlanta Georgia

Emmanouil S. Brilakis

Minneapolis Heart Institute, Minneapolis

George Dangas

Department of Cardiovascular Medicine, Mount Sinai Hospital, New York City, New York

Yves Louvard

Institut Cardiovasculaire Paris Sud, Massy

Goran Stankovic

Department of Cardiology, Clinical Center of Serbia, Belgrade

Gabriele Dubini

Laboratory of Biological Structure Mechanics (LaBS), Department of Chemistry, Materials and Chemical Engineering “Giulio Natta,” Politecnico di Milano, Milan

Francesco Migliavacca

Laboratory of Biological Structure Mechanics (LaBS), Department of Chemistry, Materials and Chemical Engineering “Giulio Natta,” Politecnico di Milano, Milan

Ghassan S. Kassab

California Medical Innovation Institute, San Diego, California

Elazer R. Edelman

Institute for Medical Engineering and Science, Massachusetts Institute of Technology, Boston, Massachusetts

Claudio Chiastra

PoliToBIOMed Lab, Department of Mechanical and Aerospace Engineering, Politecnico di Torino, Turin

Yiannis S. Chatzizisis (ychatzizisis@icloud.com)

Cardiovasclar Biology and Biomechanics Laboratory, Cardiovascular Division, University of Nebraska Medical Center, Omaha, Nebraska

---

Research Article

Keywords: Coronary artery, Stent, Three-dimensional reconstruction, Optical coherence tomography, Micro-computed tomography, Computational fluid dynamics

Posted Date: February 1st, 2021

DOI: https://doi.org/10.21203/rs.3.rs-154558/v1

3D Reconstruction of Coronary Artery Stents from Optical Coherence Tomography: *Experimental Validation and Clinical Feasibility*

Wei Wu, PhD[1*]; Behram Khan, MBBS[1*]; Mohammadali Sharzehee, PhD[1]; Shijia Zhao, PhD[1]; Saurabhi Samant, MBBS[1]; Yusuke Watanabe, MD[2]; Yoshinobu Murasato, MD, PhD[3]; Timothy Mickley, BSc[4]; Andrew Bicek, PhD[4]; Richard Bliss, PhD[5]; Francesco Burzotta, MD[6]; Habib Samady, MD[7]; Emmanouil S. Brilakis, MD, PhD[8]; George Dangas, MD, PhD[9]; Yves Louvard, MD[10]; Goran Stankovic, MD[11]; Gabriele Dubini, PhD[12]; Francesco Migliavacca, PhD[12]; Ghassan S. Kassab, PhD[13]; Elazer R. Edelman, MD, PhD[14]; Claudio Chiastra, PhD[15]; Yiannis S. Chatzizisis MD, PhD[1#]

[1]Cardiovasclar Biology and Biomechanics Laboratory, Cardiovascular Division, University of Nebraska Medical Center, Omaha, Nebraska, USA
[2]Department of Cardiology, Teikyo University Hospital, Tokyo, Japan
[3]Department of Cardiology, National Hospital Organization Kyushu Medical Center, Fukuoka, Japan
[4]Boston Scientific Inc, Hamel, Minnesota, USA
[5]Medtronic Inc, San Francisco, California, USA
[6]Department of Cardiovascular Sciences, Fondazione Policlinico Universitario A. Gemelli IRCCS Università Cattolica del Sacro Cuore, Rome, Italy
[7]School of Medicine, Emory University, Atlanta Georgia, USA
[8]Minneapolis Heart Institute, Minneapolis, USA
[9]Department of Cardiovascular Medicine, Mount Sinai Hospital, New York City, New York, USA
[10]Institut Cardiovasculaire Paris Sud, Massy, France
[11]Department of Cardiology, Clinical Center of Serbia, Belgrade, Serbia
[12]Laboratory of Biological Structure Mechanics (LaBS), Department of Chemistry, Materials and Chemical Engineering "Giulio Natta," Politecnico di Milano, Milan, Italy
[13]California Medical Innovation Institute, San Diego, California, USA.
[14]Institute for Medical Engineering and Science, Massachusetts Institute of Technology, Boston, Massachusetts, USA
[15]PoliTo^{BIO}Med Lab, Department of Mechanical and Aerospace Engineering, Politecnico di Torino, Turin, Italy

[*]The first two authors contributed equally

Word Count: 2,911

Funding Source: National Institutes of Health (R01 HL144690)

Disclosures: Yiannis S. Chatzizisis has received consulting/speaker honoraria, advisory board fees and research grant from Boston Scientific and research grant from Medtronic. He holds a provisional patent entitled "Computational simulation platform for planning of interventional procedures" (#19086P). Emmanouil S. Brilakis: Consulting/speaker honoraria from Abbott Vascular, American Heart Association (associate editor Circulation), Amgen, Biotronik, Boston Scientific, Cardiovascular Innovations Foundation (Board of Directors), CSI, Elsevier, GE Healthcare, InfraRedx, Medtronic, Siemens, and Teleflex; research support from Regeneron and

Siemens. Shareholder: MHI Ventures. Francesco Burzotta: Speaker honoraria from Medtronic, Abbott and Abiomed. Timothy Mickley and Andrew Bicek are employees of Boston Scientific Inc. Richard Bliss is employee of Medtronic Inc. All other authors have no relevant conflict of interests to disclose.

Corresponding Author:
Yiannis S. Chatzizisis, MD, PhD, FACC
Cardiovascular Biology and Biomechanics Laboratory
Cardiovascular Division, University of Nebraska Medical Center
982265 Nebraska Medical Center, Omaha, NE, 68198 USA
Tel: (402) 559-5156
Fax: (402) 559-8355
E-mail: ychatzizisis@icloud.com

ABSTRACT

The structural morphology of stents (e.g. expansion, lumen scaffolding, strut apposition, tissue protrusion, side branch jailing, strut fracture), and the local hemodynamic environment after stent deployment in coronary arteries are key determinants of procedural success and subsequent clinical outcomes. High-resolution intracoronary imaging has the potential to enable the geometrically correct 3D reconstruction of coronary stents. The aim of this work was to present a novel algorithm for 3D stent reconstruction of coronary artery stents by OCT and angiography, and test experimentally its accuracy, reproducibility, clinical feasibility and ability to perform CFD studies. Our method has the following steps: 3D lumen reconstruction by OCT and angiography, stent strut segmentation on OCT images, packaging, rotation and straightening of the segmented struts, and planar unrolling of the segmented struts, planar stent wireframe reconstruction, rolling back of the planar stent wireframe to the 3D reconstructed lumen, and stent volume reconstruction. We tested the accuracy and reproducibility of our method in stented patient-specific silicone models using micro computed tomography and stereoscopy as reference. The clinical feasibility and CFD studies were performed in clinically stented coronary bifurcations. Our experimental and clinical studies showed that our proposed algorithm can reproduce the complex stent configuration in space with high precision and reproducibility. Furthermore, our studies showed that the algorithm is feasible in clinical cases with stents deployed in diseased, bifurcated coronary arteries, enabling CFD studies to assess the hemodynamic environment. Notably, the high accuracy of our algorithm was consistent across different stent designs and diameters. Our method coupled with patient-specific CFD studies can facilitate stenting optimization, training in stenting techniques, and stent research and development.

Keywords: Coronary artery; Stent; Three-dimensional reconstruction; Optical coherence tomography; Micro-computed tomography; Computational fluid dynamics

INTRODUCTION

Coronary artery stents have revolutionized the field of interventional cardiology. The structural morphology of stents (e.g. expansion, lumen scaffolding, strut apposition, tissue protrusion, side branch jailing, strut fracture), and the local hemodynamic environment after stent deployment in coronary arteries are key determinants of procedural success and subsequent clinical outcomes.[1-7] High resolution intracoronary imaging with optical coherence tomography (OCT) and high definition intravascular ultrasound (IVUS) has been indispensable in stenting optimization.[8] Even though the cross-sectional imaging of deployed stents by OCT or IVUS provides important information on stent morphology, it does not reveal the global spatial distribution of the stent in relation to the lumen and side branches and does not provide any information on the local hemodynamic environment within the stent (macroenvironment) and around the stent struts (microenvironment). Although the commercial OCT console provides 3D rendering of the stent and lumen in a straight line, the true 3D configuration of stent and lumen cannot be appreciated and the operator has no access to the raw geometrical data, and therefore, cannot use them for further analysis or computational fluid dynamics (CFD). In this context, a platform for precise three-dimensional (3D) reconstruction of coronary stents, combined with 3D reconstruction of the arterial lumen, may unlock a wide spectrum of information, facilitating stenting optimization at the cardiac catheterization laboratory, patient-specific computational stenting simulations, and research and development of new stent technology and stenting techniques. To the best of our knowledge, there have been very few attempts for OCT-based 3D reconstruction of coronary stents.[9-13] These studies had several limitations related to insufficient validation, lack of clinical feasibility, and use of older generation stent designs deployed in straight lumen geometries.

The aim of this work was to build upon the current state-of-the-art and accomplish the following: **i)** Present a novel algorithm for 3D stent reconstruction of coronary artery stents, **ii)** Test experimentally the accuracy (at strut level) and reproducibility of the algorithm in patient-specific silicone coronary artery models, **iii)** Test the feasibility of the algorithm in diseased coronary artery bifurcations taken from patients, and **iv)** Test the feasibility of performing CFD studies in stent models 3D reconstructed by our algorithm. Notably, in this study we used stents from different vendors to highlight the versatility of our method.

METHODS

All methods were carried out in accordance with the relevant guidelines and regulations. The OCT and angiography data used in the experimental and clinical studies of this work were obtained from the PROPOT trial (randomized trial of the proximal optimization technique in coronary bifurcation lesions). The study was approved by the ethics committee of Teikyo University (IRB approval number 15-159-2) and informed consent was obtained from all subjects.

Experimental Studies

Experimental Coronary Artery Models, Flow Chamber Studies and Imaging Procedures: Four patient-specific silicone models of coronary artery lumen were created (**Figure 1**), using our in-house technique as previously described.[14] We selected both straight and curved coronary artery segments. In brief, the 3D lumen geometries were created in 3D CAAS Workstation 8.2 (Pie medical imaging, Maastricht, The Netherlands) using two angiographic projections. Negative molds were designed according to the geometries and were 3D printed with acrylonitrile butadiene styrene. Polydimethylsiloxane was mixed with its curing agent and then poured into the dry clean

molds. After curing, the silicone models were moved to an acetone beaker to dissolve the acrylonitrile butadiene styrene material. A small plastic marker was embedded in the silicone models to facilitate the correct orientation of the segmented OCT frames as described below.

The silicone models were placed in a custom-made flow chamber and a bioreactor circuit was connected to the inlet and outlet of the flow chamber, allowing circulation at a steady flow rate of 100 ml/min at room temperature. Three different widely used second generation stents (Synergy, Boston Scientific, Maple Grove, MN, USA; Resolute Onyx and Resolute Integrity, Medtronic, San Francisco, California, USA) with diameters ranging from 2.5 mm to 4.0 mm were directly implanted into the silicone models (**Table 1**). Post dilatations were not performed to assess the ability of our method to reproduce possible strut malapposition.

The stented silicone models were imaged with angiography at two projections with at least 30^{o} difference in viewing angles. OCT imaging of the stented models was obtained using the OPTIS Integrated System (Abbott, Chicago, IL, USA). The OCT catheter (Dragonfly, Optis Imaging Catheter) was advanced through a 6F guiding catheter and pulled back (automatic triggering by saline without contrast) at a speed of 18 mm/s (distance between frames at 0.1 mm) for models 1, 2, and 4, and at a speed of 36 mm/s (distance between frames at 0.2 mm) for model 3.

3D Reconstruction of Silicone Lumen: The technique for semi-automatic 3D reconstruction of the silicone lumen was previously described[14] and summarized in **Table 2**. Briefly, the lumen centerline was generated from two angiographic views (CAAS, Pie Medical Imaging BV, Maastricht, Netherlands; and VMTK, Orobix, Bergamo, Italy), and served as the backbone of the lumen reconstruction. The lumen contours from the segmented OCT images (EchoPlaque 4.0, INDEC Medical System, Los Altos, CA, USA) were aligned along the centerline and oriented

using the marker as reference. The aligned lumen contours were finally lofted to build the 3D lumen surface.

OCT Strut Segmentation and Planar Stent Flattening: The steps for OCT segmentation and planar stent flattening are illustrated in **Figure 2**. In each OCT frame used for the lumen reconstruction, we manually identified the stent contours and strut points (**Figures 2a, b**). The segmented stent contours and strut points were imported into Grasshopper 3D, a visual programming language and environment that runs within Rhinoceros 3D (Robert McNeel & Associates, Seattle, USA). Then they were packaged in a straight line along the OCT catheter center, rotated at the same angle with the corresponding lumen contour, and straightened taking the centroid of the distal stent contour as reference (**Figures 2c, d**). Finally, the stent contours and strut points were unrolled on a 2D plane (**Figures 2e, f**).

Planar Reconstruction of Stent Wireframe*:* Following the planar flattening of stent struts, the 2D stent wireframe was reconstructed according to the corresponding planar computer-aided wireframe of the stent. The planar computer-aided designs of the stents were kindly provided by the stent manufacturers (**Figures 3a, e**). The stent links were marked with circles and numbered in an ascending order starting from the proximal or distal stent edge. The flattened strut points were connected with lines according to the following rules: **i**) The ends of the lines should be at the "peak" or "valley" of the points, **ii**) The location and the sequence of the links (where the lines are connected) must be consistent with the planar computer-aided design of the stent, **iii**) At the zone of missing strut points due to wire shadow, the operator bridge the gaps using the pattern of the "peaks" and "valleys" of the planar stent wireframe as reference, and **iv**) At the contour side boundaries, the lines must be repeated to maintain the stent structure continuity.

3D Stent Reconstruction*:* The generated planar stent wireframe was rolled back in space and rounded at the peaks, using the 3D reconstructed lumen model as backbone (**Figures 3c, f**). The final stent volume was created by extruding the stent sections (circular for ONYX and Itegrity, and rectangular for SYNERGY) along the 3D reconstructed stent geometry.

Micro-computed Tomography (μCT) and Stereoscopic Imaging: The μCT and stereoscopic imaging of the stented silicone models were used as reference for the validation of the stent reconstruction algorithm. μCT imaging (Skyscanner 1172 version 1.5) was performed with the following parameters: Image pixel size 26.94 μm, voltage 100 kV, current 100 μA, and slice thickness 27 μm. The stented models were 3D reconstructed from μCT images (Mimics 22.0, Materialise, Leuven, Belgium), and smoothened (Meshmixer, Autodesk Research, New York, NY, USA). Stereoscopic imaging was performed with an Olympus SZX16 camera (Tokyo, Japan) using a 6X magnification factor.

Experimental Validation of the 3D Stent Reconstruction Algorithm: The OCT-based 3D reconstructed stents were compared to the μCT reconstructed ones and stereoscope imaging, using μCT and stereoscopy as references. For the quantitative comparisons between OCT-based and μCT-based reconstructions, the following metrics were used: **i)** Stent length, **ii)** Mean stent diameter (MSD), defined as the average stent diameter of serial cross-sections every 0.1 mm along the stent length, **iii)** Stent shape, calculated by the ellipse ratio, i.e. the ratio of the maximum distance between the two furthest points of the stent cross-sectional circumference (distance X), and the maximum distance perpendicular to distance X (distance Y), and **iv**) Malapposition, calculated as the maximum distance between stent struts and lumen. To minimize possible biases, different operators performed the 3D reconstruction from OCT, 3D reconstruction from μCT, and comparison between OCT- and μCT-based models.

Reproducibility: To calculate the reproducibility of the OCT-based 3D reconstruction method, the stents were 3D reconstructed by two independent operators. The reconstructed stents were compared in terms of MSD and stent shape, as above.

Clinical Studies

Clinical Feasibility, Processing Times, and CFD Studies: The clinical feasibility and processing times of our stent reconstruction method were assessed in n=3 patient coronary artery bifurcations with varying degrees of disease (**Supplementary Table 1**). All these cases underwent stenting with one stent. OCT and angiography data were acquired according to the imaging protocols mentioned above. Both lumen and stent were 3D reconstructed following the steps of our proposed algorithm. To assess the time-efficiency of our stent reconstruction method, we calculated the processing time for each step in all three clinical cases.

Also, we assessed the feasibility of CFD studies in stents reconstructed with our method. The fluid domain was discretized into tetrahedral elements for the lumen (element size = 0.15 mm) and the stent (element size = 0.02 mm). Velocity inlet and outflow ratios were employed for the boundary conditions in which pulsatile flow of a human left coronary artery was used[15], and the inlet velocity was tuned according to inlet diameter.[16] Outflow ratio was determined based on the diameter ratio of left anterior descending and left circumflex arteries.[16] Extensions of 10-diameter were added into the inlet and outlet sections to minimize the effect of boundary conditions. We considered blood as Newtonian fluid with density of 1,050 kg/m^3 and dynamic viscosity of 0.0035 Pa s. The flow was considered to be laminar as the maximum Reynolds numbers of all cases at the maximum flow rate at the vessel inlet were less than the threshold of 2,300. The simulations were performed for n=3 cardiac cycles using a time step of 0.01 s, and only the last cycle results are

shown. We calculated the time-averaged wall shear stress (TAWSS) using the following equation: $TAWSS = \frac{1}{T}\int_0^T |\tau_w| dt$, τ_w is the wall shear stress.

Statistical Analyses

Statistical analyses were performed with the statistical package GraphPad Prism 8.0 (GraphPad Inc., San Diego, CA, USA). Continuous variables are expressed as mean±SEM. For the validation and reproducibility studies we used Bland-Altman analysis.

RESULTS

Experimental Validation

Stent Morphology: All experimental stent models (n=4) were successfully 3D reconstructed and compared to the corresponding μCT reconstructed models and stereoscopy imaging (**Figures 4a-d**). As indicated by the boxes, there was good agreement in terms of the location of stent links between OCT-reconstructed stents and μCT and stereoscopy, suggesting the robustness of our method to reproduce the real stent geometry even at the strut level.

Stent Size, Shape and Malapposition: There was a high agreement in stent length and MSD between the 3D reconstructed stents by OCT vs. μCT (**Table 3** for lengths, **Figure 5a** for MSD). Bland Altman analysis of the MSD between OCT- and μCT-reconstructed stents revealed a very small mean difference of 0.001 mm (-0.12 to 0.12 mm, with 95% confidence intervals). Similarly, the stent shapes were very close between OCT and μCT reconstructions, yielding a mean difference of ellipse ratios of 0.2 (-0.02 to 0.05; **Figure 5b**). Furthermore, our stent reconstruction method reproduced the severity of strut malapposition with high precision (**Figure 4e)**. These results strongly suggest the high accuracy of our method.

***Reproducibility**:* As shown in **Figure 6a**, overlapping of the 3D reconstructed stents by two different operators, yielded high inter-observer reproducibility of our methodology. Quantitative comparison of MSD of reconstructed stent models by two different operators showed that the curves of MSD along the stent length were almost overlapped (**Figure 6b**). Bland-Altman analysis revealed minimum mean differences in MSD of 0.002 mm (-0.019 to 0.013 mm), suggesting the very high reproducibility of the proposed stent reconstruction method.

Clinical Feasibility and CFD Studies

In all clinical cases (n=3), the stents were successfully 3D reconstructed along with the corresponding coronary bifurcation lumens. The reconstructed stented bifurcations were qualitatively compared with the angiograms and showed good agreement in size and shape **(Figures 7a, b)**. The processing times for each step, from image processing to final 3D lumen and stent reconstruction, are summarized in **Table 4**. The average time for 3D reconstruction of stents was 177±42 minutes, with longer stents requiring more processing time.

The reconstructed stented bifurcations were meshed **(Figure 7c)**, and underwent CFD studies. **Figure 7d** shows the TAWSS distribution along the reconstructed stented bifurcation (macroenvironment). At the strut level (microenvironment), note the occurrence of disturbed flow (TAWSS and high velocity) around the malapposed struts, and at the stented carina (**Figure 8**).

DISCUSSION

In this study, we present a new methodology for the 3D reconstruction of coronary artery stents using combined imaging with OCT and angiography. We assessed **i)** The accuracy and reproducibility of the method using patient-specific silicone models of coronary arteries, and **ii)** The clinical feasibility, time-efficiency and ability to perform CFD studies using clinical

bifurcation cases. For the validation studies we used μCT and stereoscopy imaging as reference. Our studies showed that our proposed algorithm can reproduce the complex stent configuration in space with high precision at the micro-scale (strut level) and reproducibility. Furthermore, our studies showed that the algorithm is feasible in clinical cases with stents deployed in diseased, bifurcated coronary arteries, enabling CFD studies to assess the hemodynamic environment at the lumen and strut level. Notably, the high accuracy of our algorithm was consistent across three contemporary second generation stents (Synergy, Resolute Onyx, Resolute Integrity) with diameters ranging from 2.5 to 4.0 mm, supporting the versatility of our method.

To the best of our knowledge, this work overcomes several limitations of previous studies in the field and advances the current state-of-the-art. **Table 5** provides a comprehensive head-to-head comparison of our study to the previous studies[10,12,13] and available software. The commercially available OCT console (OPTIS Integrated System, Abbott, Chicago, IL, USA) provides real-time 3D reconstruction of the stent in a straight line. Using this software, the interventionalists can easily assess several stent morphological parameters like expansion, apposition, and side branch jailing at the point of care. However, the major disadvantage of the OCT console is that it cannot reconstruct the geometrically correct stent configuration, and therefore cannot be used for CFD studies. Furthermore, this software is proprietary and the raw stent geometrical data are not accessible for further stent analysis and research. In contrast to the OCT console, our method reconstructs the true geometry of the stent that can be used for CFD studies. Of note, our algorithm is free and open to the scientific community. The 3D stent reconstruction methods proposed by Maligliori et al[12] and Elliott et al[10] were based on geometrical information retrieved by OCT and μCT. Since the use of μCT was an integral part of the reconstruction method, these techniques cannot be used in the clinical setting and their value is

only for experimental research. In contrast to these two studies, in our method we used μCT only for the purpose of validation. Also, our method has direct and proven clinical applicability given that is relies on angiography and OCT only. Furthermore, Maligliori et al used older generation stents (name them here), whereas in our study we used contemporary stents (Integrity, Onyx, Synergy) of varying size. Finally, the method proposed by O'Brien et al[13], is similar to our work using OCT and angiography as the input anatomical information for the 3D stent reconstruction. In fact, this work used an automatic technique for stent strut segmentation which is advantageous compared to our manual approach. However, the work by O'Brien has some major limitations that we overcome in our study: O'Brien's work used outdated and rather simple bare metal stent designs and its performance in current drug eluting stent designs remains to be proven. We feel that the O'Brien's strut point mapping method may not be as accurate for more complex stent geometries and average quality OCT data. In contrast, our method performed well even with real world average quality OCT data. Overall, the technically innovative approach of our method, along with the systematic validation and testing of clinical feasibility using real world contemporary second generation stents, are notable advantages of our technique over the previous state-of-the-art.

Our methodology has several important technical aspects and innovations: First, it is based on a well-validated lumen reconstruction method.[14] The geometrically correct lumen reconstruction determines the location and orientation of stent contours and struts points, as well as the relative location of the stent within the lumen. Second, our approach to unroll the stent contours and strut points and reconstruct the planar stent wireframe was a critical step, enabling faster and more accurate stent reconstruction. Direct 3D reconstruction based on the 3D strut segmentation, appears to be technical challenging due to the geometrically complex distribution of strut points in space (**Figure 2**). This becomes more pertinent at the gaps induced by the wire

shadow, where the operator has difficulty in appreciating the correct 3D position of the missing strut points. In contrast, when the strut points are unrolled on a 2D plane, it is much easier for the operator to find the stent pattern and fill the gaps, especially using the 2D stent design as reference (**Figure 3**). Third, in our method, the stent links served as critical nodes for the precise planar reconstruction of the stent framework and subsequent 3D reconstruction of the stent (**Figure 3**). Finally, all the steps in our method were automatic or semi-automatic except for the manual effort to reconstruct the planar stent wireframe. Our code coordinated all these steps effectively, thereby reducing the human interaction and processing times, and improving the accuracy and reproducibility of the proposed technique.

The proposed methodology has several scientific and clinical applications. It can be used at the cardiac catheterization laboratory to inform the interventionalists on the spatial configuration of the deployed stent in relation to the main vessel lumen and side branches (when applicable), identifying areas of stent under-expansion, strut malapposition, and floating struts at the carina and side branch ostium. This information is essential for stenting optimization which is directly related to favorable clinical outcomes.[17,18] Furthermore, our method can be combined with extended reality techniques to allow high-resolution visualization of the deployed stents for educational purposes. The proposed method can enable accurate CFD and solid mechanics studies to assess the local biomechanical environment after stenting with emphasis on the strut level and the anatomically sensitive areas of bifurcations. Studies showed that areas with disturbed flow and high shear rates are associated with increased propensity to stent restenosis and thrombosis.[3,19] Identification of these hemodynamically unfavorable areas within stents may enable improved stenting optimization and clinical outcomes. Geometrically-correct stents reconstructions can also provide important feedback to the stent manufacturers on the design and performance of their

products creating opportunities for stent design optimization. Of note, our method has the potential to use other intracoronary imaging modalities, such as high definition IVUS, as input. Since the only difference between these methods is how imaging can be segmented for the stent contour and strut points, our method can reconstruct the stent with a general imaging source. The relatively simple steps of our method can allow operators without technical or engineering background (e.g., medical students, fellows) to use it, making it more widely applicable.

This study has several limitations. First, although the processing time is reasonable, it is still not fast enough. The most time-consuming steps in the process were the **i)** Semi-automatic strut segmentation on OCT images (average 60±10 min), **ii)** Manual planar reconstruction of the stent (average 87±18 min) and the data transfer between different software used for the angiography and OCT image processing (i.e., CAAS, EchoPlaque, VMTK). Our current efforts focus towards developing a fully automated strut segmentation algorithm (requiring limited manual corrective intervention), developing a smart algorithm for planar stent wireframe reconstruction (limiting the manual intervention to the absolutely challenging cases), and developing a new Grasshopper code to streamline the cross-talk between different software. We believe that with these efforts we can make our algorithm significantly faster. Second, our method requires good quality OCT images. OCT images with incomplete blood clearance and severe image artifacts would not allow the operator to identify the stent struts making the planar reconstruction of the stent wireframe quite challenging. Third, we performed CFD simulations for three patients to demonstrate the feasibility of the realistic CFD simulations. Further studies are required to simulate more clinical cases to provide inputs for clinical decision making of coronary artery stenting. Last, our technique's performance was tested in single stenting. The ability of the proposed method to reconstruct two stents deployed in bifurcations is subject of future work.

Conclusion

In conclusion, in this work we propose a new method that enables accurate, reproducible, time-efficient and clinically feasible 3D reconstruction of coronary artery stents. This method coupled with CFD studies can facilitate stenting optimization, training in stenting techniques, and stent research and development.

ACKNOWLEDGMENTS

The study was funded by the National Institutes of Health (R01 HL144690) and Dr. Vincent Miscia Cardiovascular Research Fund.

AUTHOR CONTRIBUTIONS STATEMENT

Conception and design: Y.S.C., W.W.; Acquisition of data: W.W., B.K., M.S., S.Z., S.S., Y.W., Y.M., T.M., A.B., R.B., Y.S.C.; Analysis and interpretation of data: W.W., B.K., M.S., S.Z., S.S., C.C. Y.S.C.; Manuscript drafting and revision: Y.S.C, W.W., B.K., M.S., Y.W., F.B., H.S., E.S.B., G.D., Y.L., G.S., G.D., F.M., G.S.K., E.R.E., C.C. All authors were involved in drafting the article or revising it critically for intellectual content, and all authors approved the final version to be published.

References

1. Antoniadis, A. P. *et al.* Biomechanical Modeling to Improve Coronary Artery Bifurcation Stenting: Expert Review Document on Techniques and Clinical Implementation. *JACC: Cardiovascular Interventions* **8**, 1281-1296 (2015).
2. Chen, C. *et al.* In vivo and in vitro evaluation of a biodegradable magnesium vascular stent designed by shape optimization strategy. *Biomaterials* **221**, 119414 (2019).
3. Chiastra, C. *et al.* Computational replication of the patient-specific stenting procedure for coronary artery bifurcations: From OCT and CT imaging to structural and hemodynamics analyses. *Journal of Biomechanics* **49**, 2102-2111 (2016).
4. Foin, N. *et al.* Incomplete stent apposition causes high shear flow disturbances and delay in neointimal coverage as a function of strut to wall detachment distance: implications for the management of incomplete stent apposition. *Circ Cardiovasc Interv* **7**, 180-189 (2014).
5. Kolandaivelu, K. *et al.* Stent thrombogenicity early in high-risk interventional settings is driven by stent design and deployment and protected by polymer-drug coatings. *Circulation* **123**, 1400-1409 (2011).
6. Koskinas, K. C., Chatzizisis, Y. S., Antoniadis, A. P. & Giannoglou, G. D. Role of Endothelial Shear Stress in Stent Restenosis and Thrombosis: Pathophysiologic Mechanisms and Implications for Clinical Translation. *Journal of the American College of Cardiology* **59**, 1337-1349 (2012).
7. Valeria, P. *et al.* Thrombogenicity at the jailed side branch ostia in the provisional stenting technique: insights from an in vitro model. *EuroIntervention* **14**, 826-827 (2018).
8. Räber, L. *et al.* Clinical use of intracoronary imaging. Part 1: guidance and optimization of coronary interventions. An expert consensus document of the European Association of Percutaneous Cardiovascular Interventions. *European Heart Journal* **39**, 3281-3300 (2018).
9. Bologna, M. *et al.* Automatic segmentation of optical coherence tomography pullbacks of coronary arteries treated with bioresorbable vascular scaffolds: Application to hemodynamics modeling. *PLoS One* **14**, e0213603-e0213603 (2019).
10. Elliott, M. R. *et al.* Establishment of an Automated Algorithm Utilizing Optical Coherence Tomography and Micro-Computed Tomography Imaging to Reconstruct the 3-D Deformed Stent Geometry. *IEEE Transactions on Medical Imaging* **38**, 710-720 (2019).
11. Lin, C. Y., Veneziani, A. & Ruthotto, L. Numerical methods for polyline-to-point-cloud registration with applications to patient-specific stent reconstruction. *International Journal for Numerical Methods in Biomedical Engineering* **34**, e2934 (2018).
12. Migliori, S. *et al.* A framework for computational fluid dynamic analyses of patient-specific stented coronary arteries from optical coherence tomography images. *Med Eng Phys* **47**, 105-116 (2017).
13. O'Brien, C. C. *et al.* Constraining OCT with Knowledge of Device Design Enables High Accuracy Hemodynamic Assessment of Endovascular Implants. *PLoS One* **11**, e0149178 (2016).
14. Wu, W. *et al.* 3D reconstruction of coronary artery bifurcations from coronary angiography and optical coherence tomography: feasibility, validation, and reproducibility. *Scientific Reports* **10**, 18049 (2020).
15. Davies, J. E. *et al.* Evidence of a dominant backward-propagating "suction" wave responsible for diastolic coronary filling in humans, attenuated in left ventricular hypertrophy. *Circulation* **113**, 1768-1778 (2006).
16. van der Giessen, A. G. *et al.* The influence of boundary conditions on wall shear stress distribution in patients specific coronary trees. *J Biomech* **44**, 1089-1095 (2011).

17. Cook, S. *et al.* Impact of incomplete stent apposition on long-term clinical outcome after drug-eluting stent implantation. *European Heart Journal* **33**, 1334-1343 (2012).
18. Im, E. *et al.* Incidences, Predictors, and Clinical Outcomes of Acute and Late Stent Malapposition Detected by Optical Coherence Tomography After Drug-Eluting Stent Implantation. *Circulation: Cardiovascular Interventions* **7**, 88-96 (2014).
19. Chiastra, C. *et al.* Computational fluid dynamic simulations of image-based stented coronary bifurcation models. *Journal of The Royal Society Interface* **10**, 20130193 (2013).

Figure 1. Patient-specific silicone models. In each model from left to right: angiography, computer-aided design before stenting, OCT-reconstructed lumen after stenting and stereoscopy images of the final stented models. In stereoscopy images, the arrows indicate the markers used as reference for the orientation of the 3D reconstructed lumen.

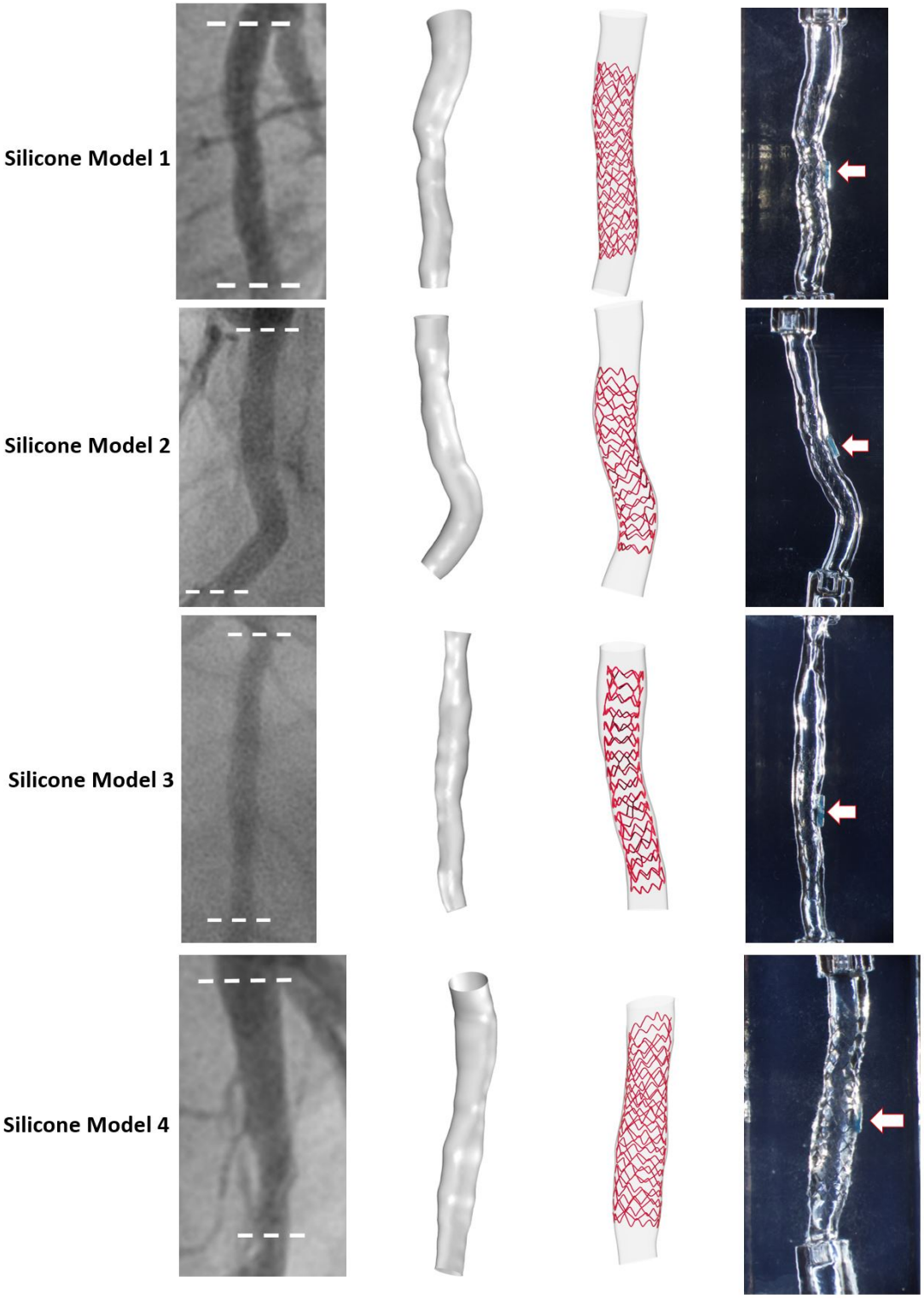

Figure 2. OCT stent segmentation and planar unrolling. **(a)** Segmented stent contour (white circle) and **(b)** strut points (white boxes), and arrows indicate the marker, **(c)** Packaging of segmented stent contours and strut points in space, **(d)** Rotation and straightening of the packaged stent contours and strut points, **(e)** and **(f)** Planar unfolding (stent contours in red, stent strut points in green). The purple strut points were added to show the continuity of stent structure. In **(e)** and **(f)** note the zone of missing strut points corresponding to the wire artifact. **(a-e)** correspond to Onyx stent and **(f)** to Synergy stent.

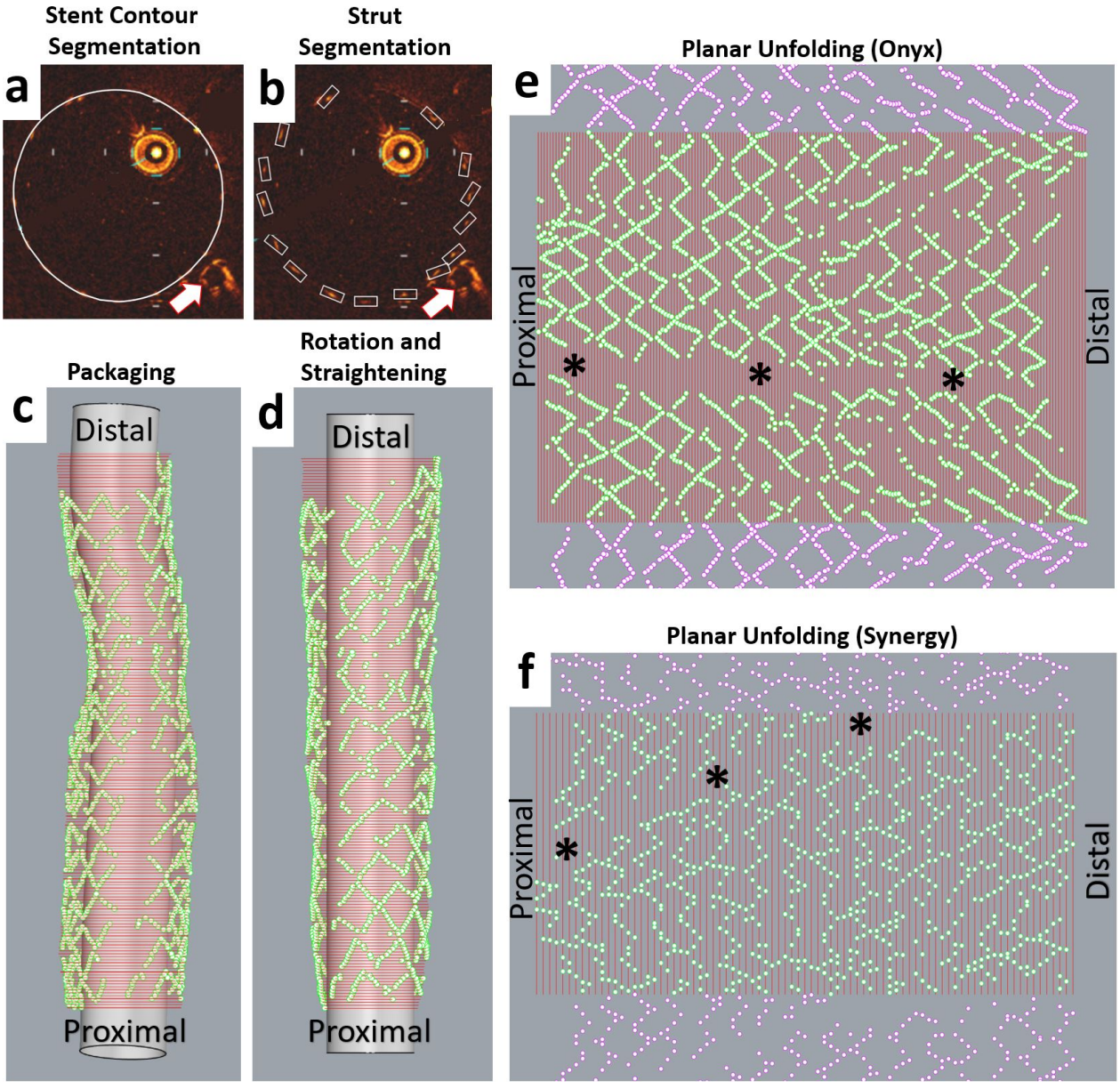

Figure 3. Planar stent wireframe reconstruction and rolling back to space. Planar computer-aided design of **(a)** Onyx stent and **(d)** Synergy stent with the boundaries delineated by red lines. Planar stent reconstruction (black lines) of **(b)** Onyx and **(e)** Synergy using the unrolled stent strut points and computer-aided stent designs as reference. The numbers and circles in **(b)** and **(e)** indicate the location of stent links. Note the extension of black lines beyond the stent boundaries, to show the stent continuity for the next steps. Rolling back of 2D reconstructed **(c)** Onyx stent wireframe and **(f)** Synergy stent wireframe and volume creation: **(c1 and f1)** 3D reconstructed lumen used as backbone for the 3D stent reconstruction. The red points are segmented stent strut points, **(c2 and f2)** 3D rolling-back of 2D reconstructed stent wireframe (blue) following the lumen shape, **(c3 and f3)** Original strut points (red) overlapped on the rolled back stent wireframe, **(c4 and f4)** Final stent volume generated from stent wireframe. In **(c2, c3, f2 and f3)** a tube was added inside the stent wireframe for better visualization. Stent designs were kindly provided by the stent manufacturers.

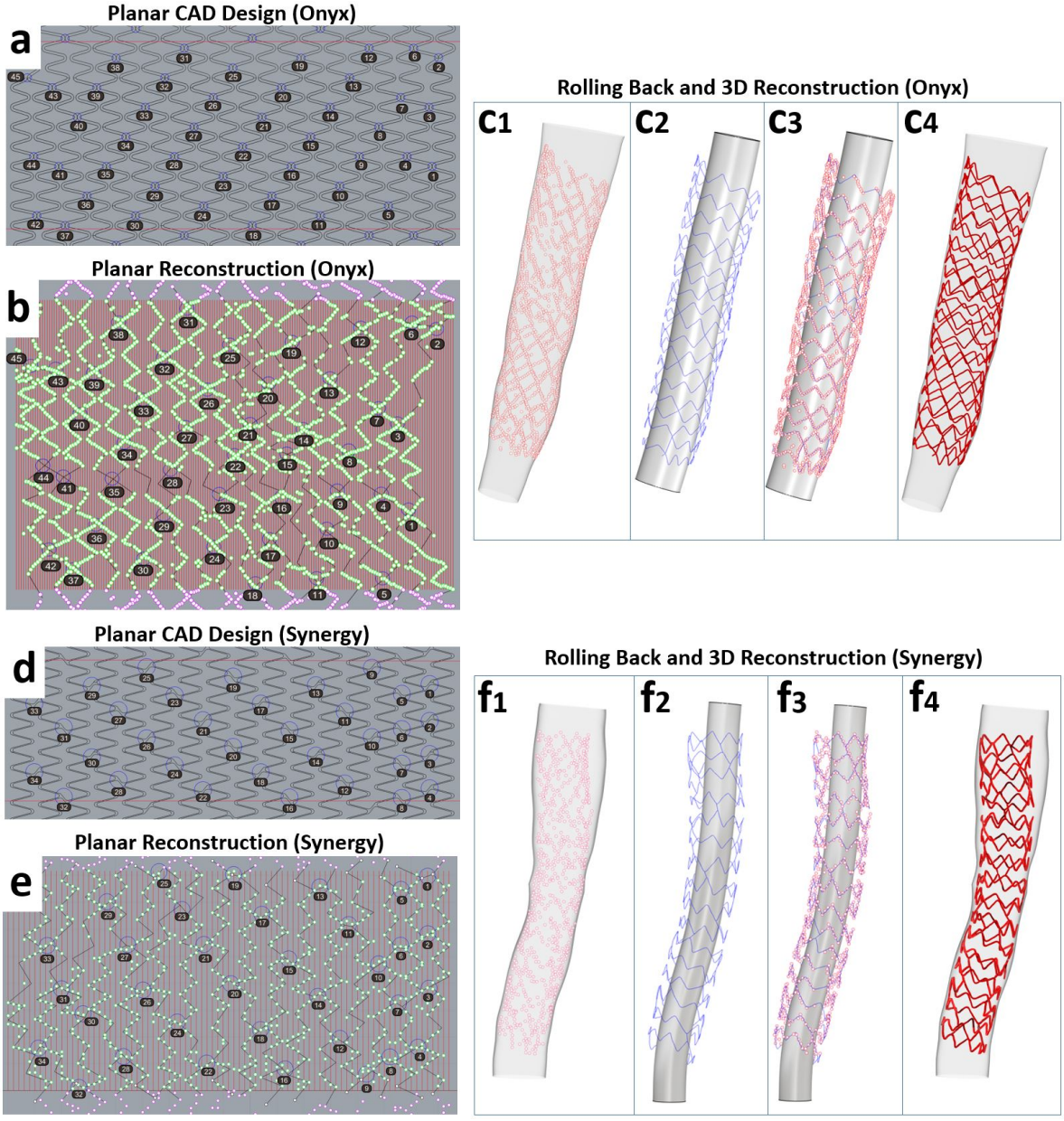

Figure 4. Qualitative experimental validation of stent reconstruction method against μCT and stereoscopic imaging. **(a-d)** Note the agreement in the link position (blue boxes in OCT-stent reconstructions and red boxes in μCT-reconstruction and stereoscopy). In OCT and μCT-based reconstructed models, a tube was inserted for better visualization, whereas in stereoscopy images a small balloon was inflated in very low pressures for better visualization, **(e)** Malapposed struts in OCT stent reconstruction at the same location and magnitude compared to μCT.

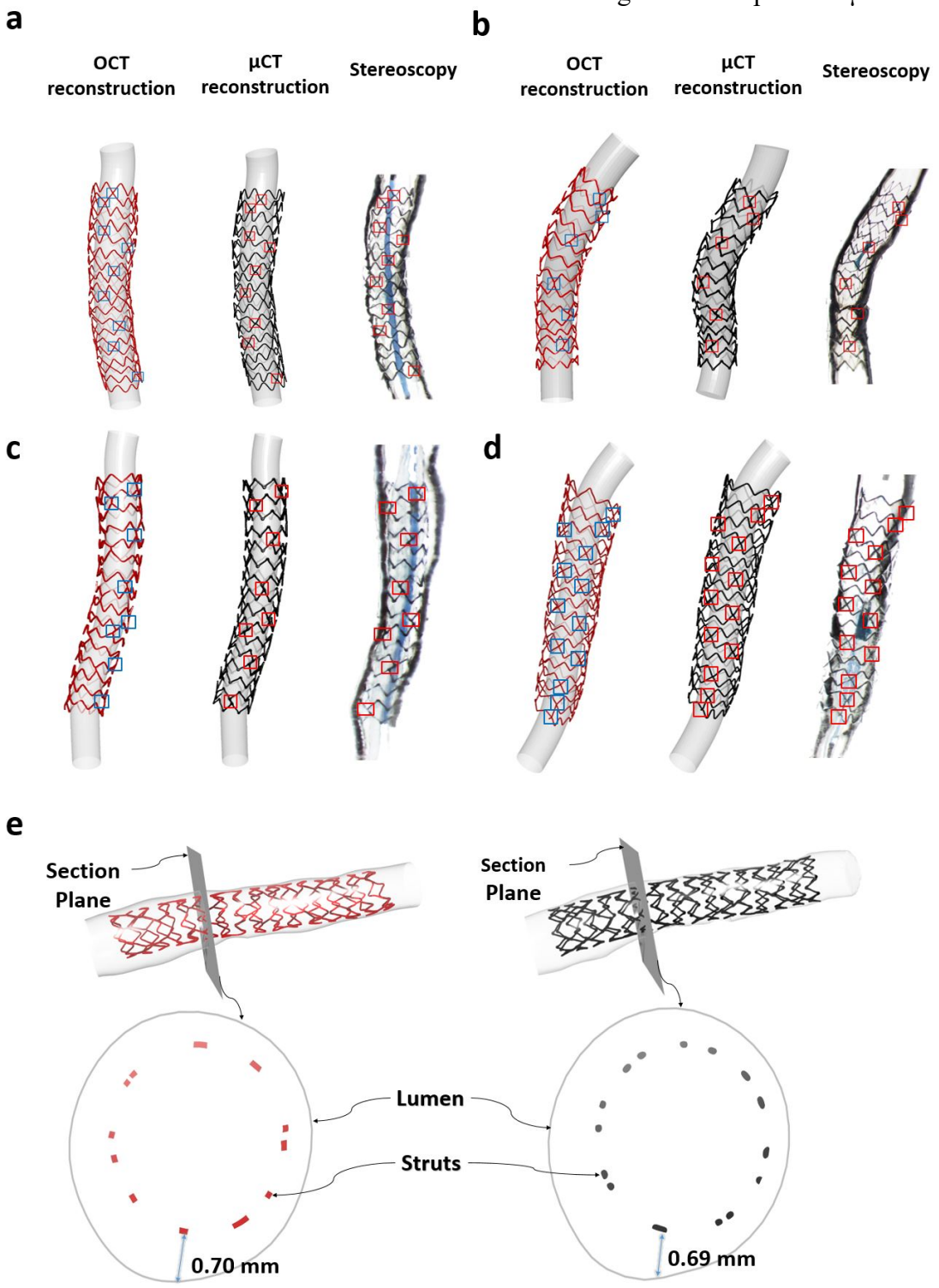

Figure 5. Quantitative experimental validation of stent reconstruction method against µCT. **(a)** Stent size measured by mean stent diameter (MSD), **(b)** Stent shape measured by ellipse ratio

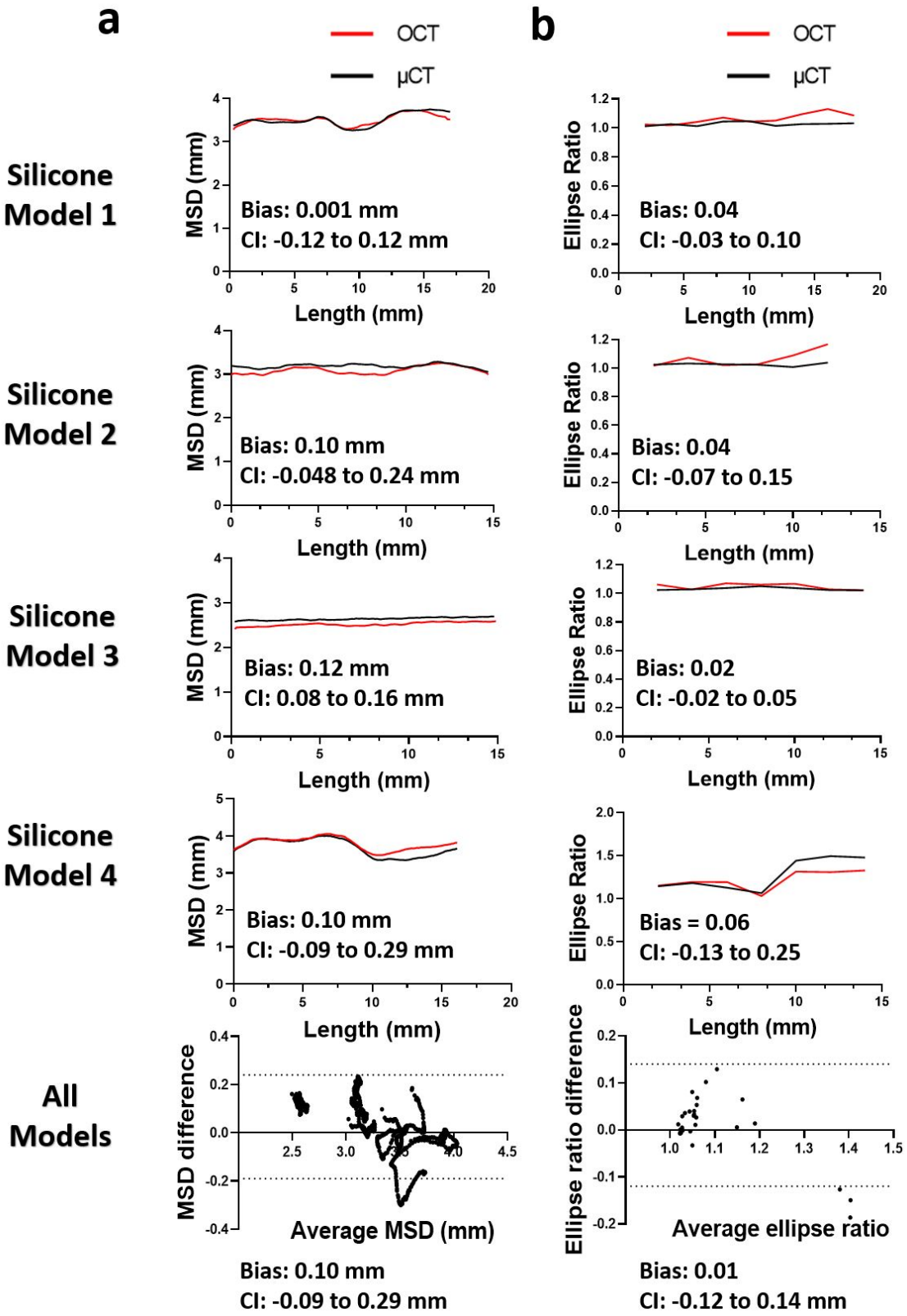

Figure 6. Inter-observer reproducibility of OCT-based stent reconstructions. **(a)** Qualitative agreement by overlapping the two reconstructed stents. **(b)** Quantitative agreement for each model (MSD, mean stent diameter) and overall agreement using Bland Altman analysis

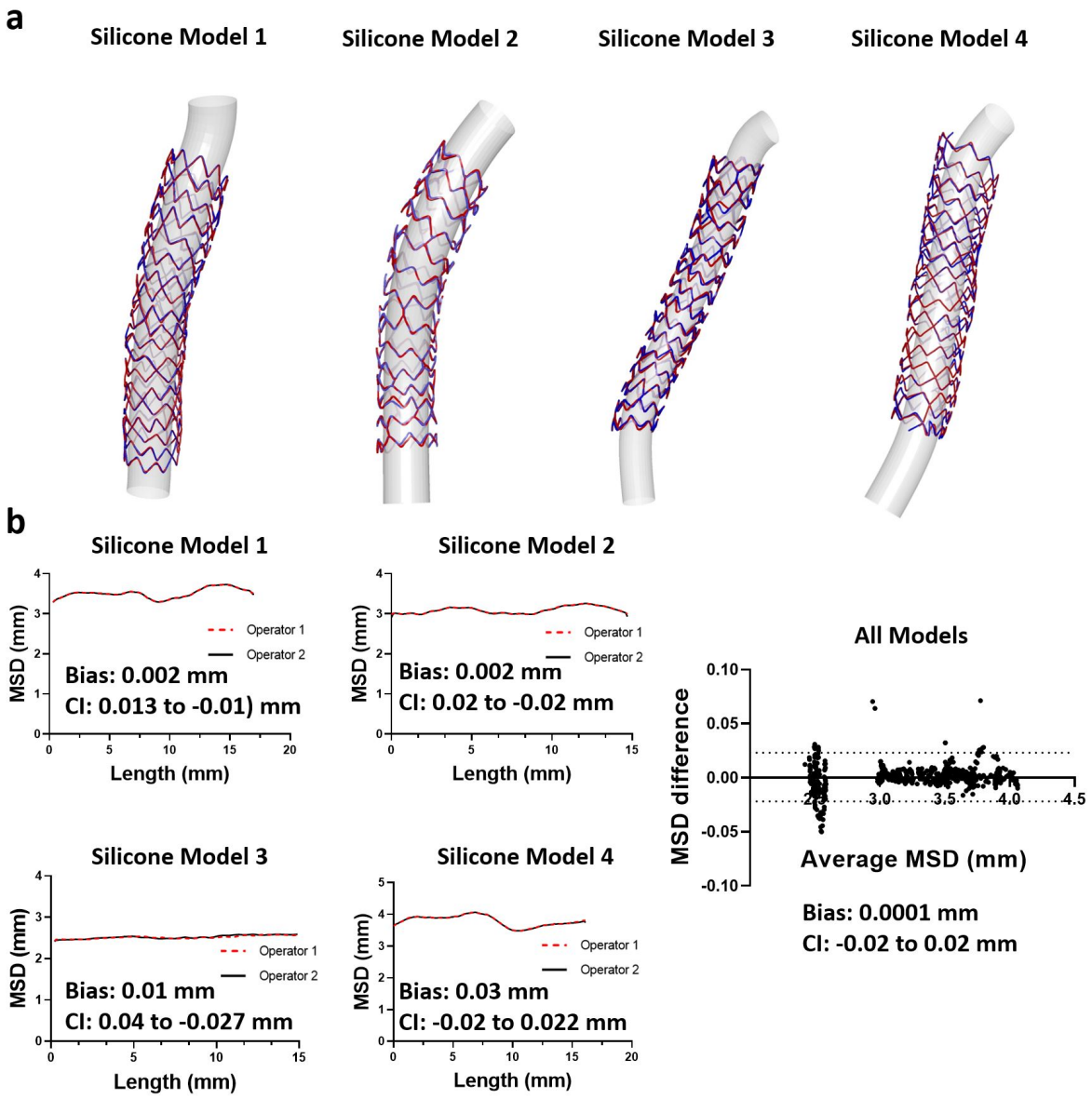

Figure 7. Clinical feasibility of the proposed 3D stent reconstruction method. **(a)** Invasive coronary angiography post stenting, **(b)** 3D lumen and stent reconstruction. Note the qualitative agreement to angiography, **(c)** Lumen and stent meshing, **(d)** CFD analysis depicting the time-averaged wall shear stress (TAWSS, Pa) along the stented bifurcations.

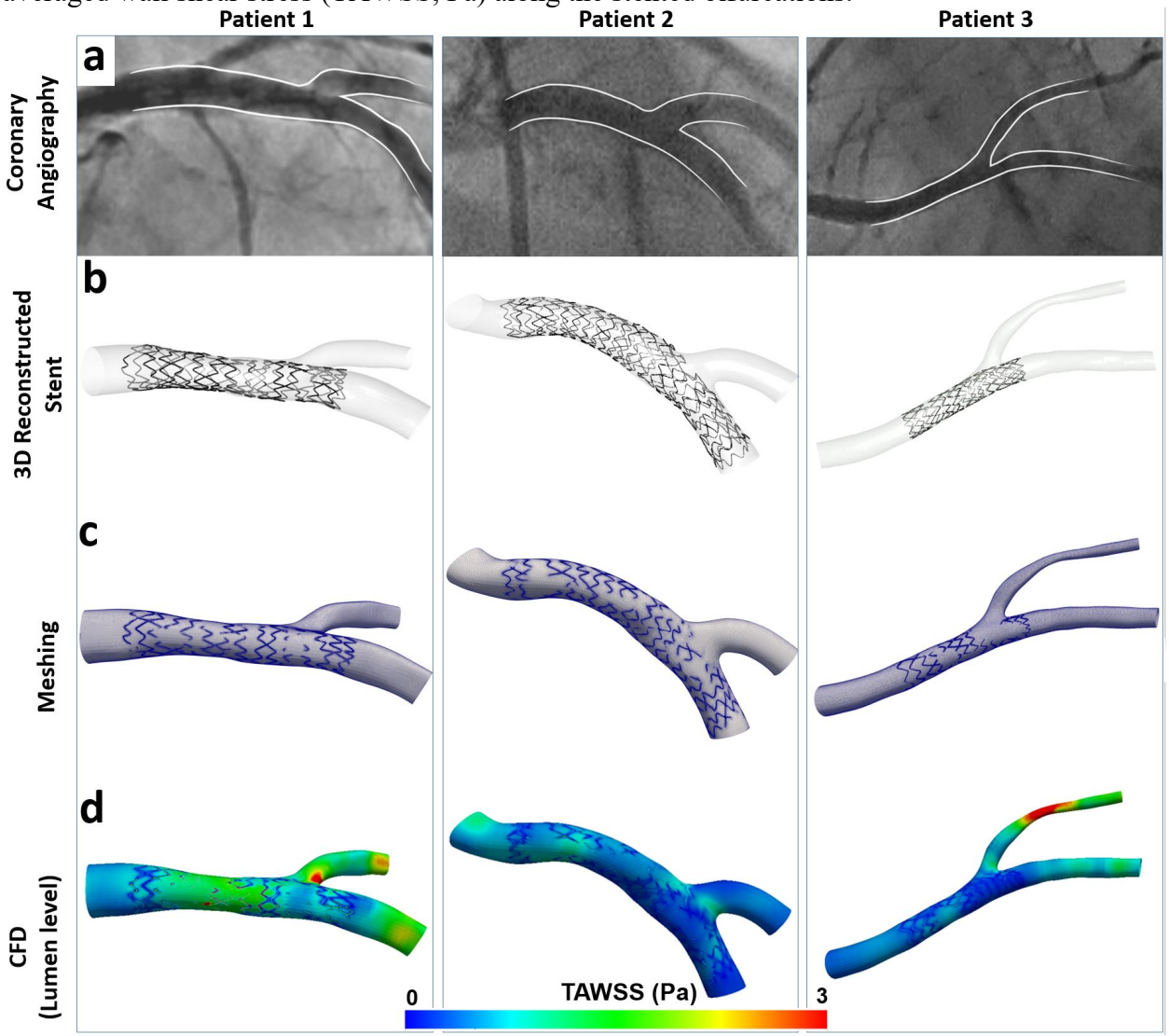

Figure 8. Examples of the calculated hemodynamic micro-environment (strut level) in patient-specific 3D reconstructed stented bifurcations (provisional stenting). **(a-c)** TAWSS around stent struts. In **(a)** note the increased shear stress on the luminal surface of a well-apposed strut, and in **(b-c)** the shear stress distribution around malapoposed struts denoted with white asterisks. In **(d)** longitudinal section showing the low velocity between the lumen and malapposed struts (white asterisks). **(e-g)** TAWSS distribution at the ostium of the side branch. Note the struts jailing the ostium of the side branch.

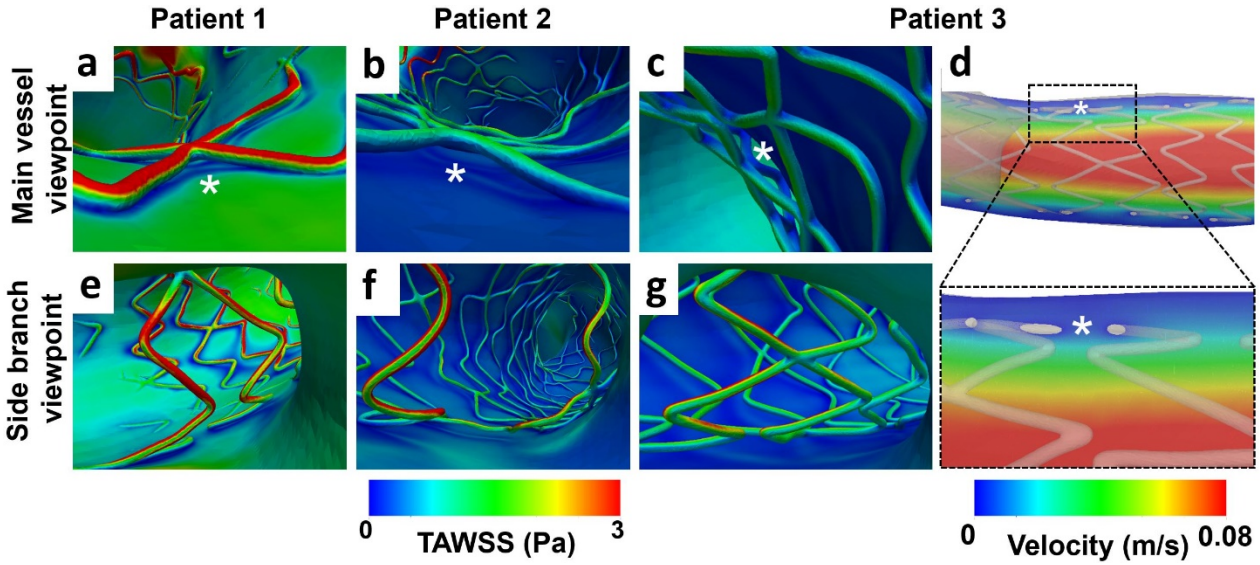

Tables

Table 1. Stent types and length measurement

	Stent	**Inflation pressure**	**OCT frame distance (mm)**
Model 1	Resolute Integrity 3.5x18 mm	16 atm	0.1
Model 2	Synergy 3.0x16 mm	18 atm	0.1
Model 3	Synergy 2.5x16 mm	18 atm	0.2
Model 4	Resolute Onyx 4.0x18 mm	16 atm	0.1

Table 2. Steps of the proposed method for 3D stent reconstruction

1. 3D lumen reconstruction	2.1. Stent contour and strut point segmentation in OCT images 2.2. Packaging, rotation, straightening and planar unrolling of strut points and contours 2.3. Planar stent wireframe reconstruction
3.1. Rolling back of the planar stent wireframe with the 3D reconstructed lumen as reference 3.2. Stent volume reconstruction	

Table 3. Comparison of the length of the 3D reconstructed stents by OCT and μCT

	Model 1	**Model 2**	**Model 3**	**Model 4**
Length by μCT (mm)	15.7	16.1	15.7	17.3
Length by OCT (mm)	15.8	15.7	15.8	17.3

Table 4. Processing times for 3D stent reconstruction in clinical cases (n=3)

Steps	**Time (min)**
Step 1. 3D lumen reconstruction	56±5
Step 2. 2D stent reconstruction	
1. OCT stent segmentation	60±10
2. Data importing and parameter setting	5±1
3. Frame packaging, rotation, straightening and planar flattening	5±1
4. Planar stent reconstruction	87±18
Step 3. 3D rolling back and stent volume creation	20±2
Total time for 3D stent reconstruction (excluding step 1)	**177±42**
Total time for whole process	**233±20**

Table 5. Comparison between different stent reconstruction methods

Study	Model Type	Number of Models (n)	Imaging Used	Technique for Segmentation	3D Reconstruction Technique	Processing Time	Validation Method	Clinical Feasibility	Versatility (Stent types)	CFD Analysis Done	Major Limitations
Our Study (CBBL)	In-vitro + In-vivo	7 (4 in-vitro +3 in-vivo)	OCT + Angio	Manual Segmentation (Lumen + Stent-contour + Struts)	2D manual framework + stent design; rolled back to 3D geometry	180 + min	**Qualitative metrics** Final geometry vs. µCT, stereoscopy, angiography: -Stent shape -Stent links -Strut apposition **Quantitative metrics** Final geometry vs. µCT: -MSD -Stent shape ratio -Stent length	Yes	1-Synergy 2-Onyx 3-Integrity	Yes	-Long duration of Processing time
Elliott et al[10]	In-vitro	4	OCT + µCT	Automatic Segmentation using algorithm (Struts)	3D automatic mapping of known µCT derived stent design over the strut points	30 min	**Qualitative metrics** Pre-final geometry vs. segmented strut points: -Planer stent pattern **Quantitative metrics** Pre-final geometry vs. µCT derived wire-frame. -Euclidean distance	No	1-Integrity 2-Xience Alpine	No	-No clinical applicability; µCT is required in this method. -CFD analysis not done. -Validation was not done for the final geometry.
Migliori et al[12]	In-vitro	1	OCT + µCT	Automatic Segmentation using algorithm (Lumen + Struts)	3D manual mapping of known µCT derived stent design over the strut points	NA	**Qualitative metrics** Final geometry vs. µCT: -Visual comparison. **Quantitative metrics** Segmented strut points vs. µCT -Distance between the strut points and µCT.	No	1-Multi Link 8	Yes	- No clinical applicability; µCT is required in this method -Technical complexity in 3D manual mapping of strut points especially at the region of catheter shadow - Validation was not done for the final geometry -Old stent used
O' Brien et al[13]	In-vivo	4	OCT + Angio	Automatic Segmentation using algorithm (Lumen + Struts)	3D automatic mapping of known stent design over the strut points	NA	**Quantitative metrics** Final geometry vs. Original strut points: -Displacement error between strut points and stent landmark -Diameter -Stent curvature **Qualitative metrics** Not Done	Yes	1-Small cell bare metal Stent 2-Large cell bare metal stent	Yes	-Qualitative metrics of validation not done. -Old Stents used -Validated against automatic strut segmentation which itself has its limitations.
OCT Console	In-vitro + In-vivo	Not applicable	OCT	Automatic Segmentation using algorithm (Lumen + Struts)	Not Done		Unknown	No	All commercially available stents	No	-Virtual straight geometry cannot be used for CFD. -Proprietor

Figures

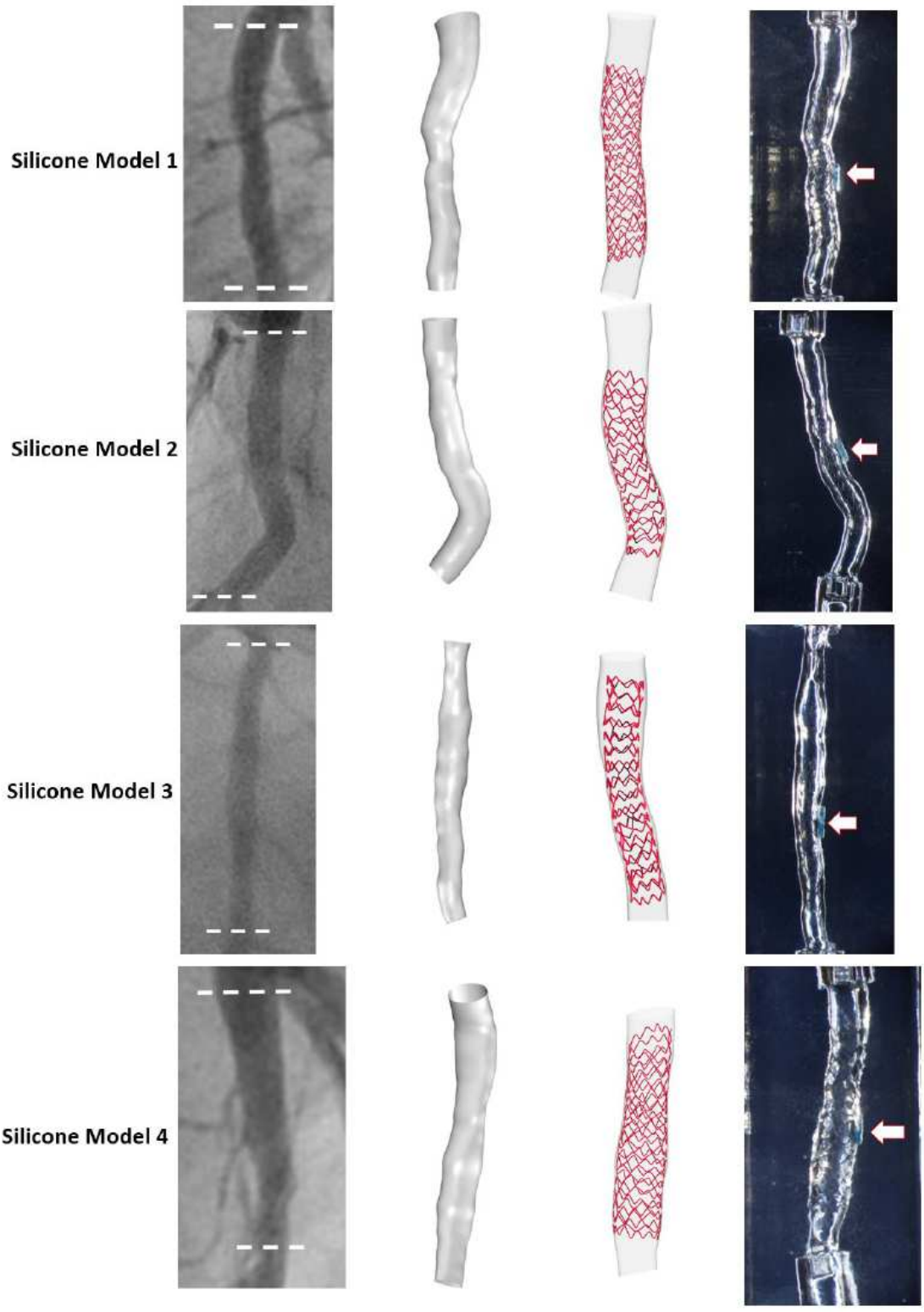

Figure 1

Patient-specific silicone models. In each model from left to right: angiography, computer-aided design before stenting, OCT-reconstructed lumen after stenting and stereoscopy images of the final stented

models. In stereoscopy images, the arrows indicate the markers used as reference for the orientation of the 3D reconstructed lumen.

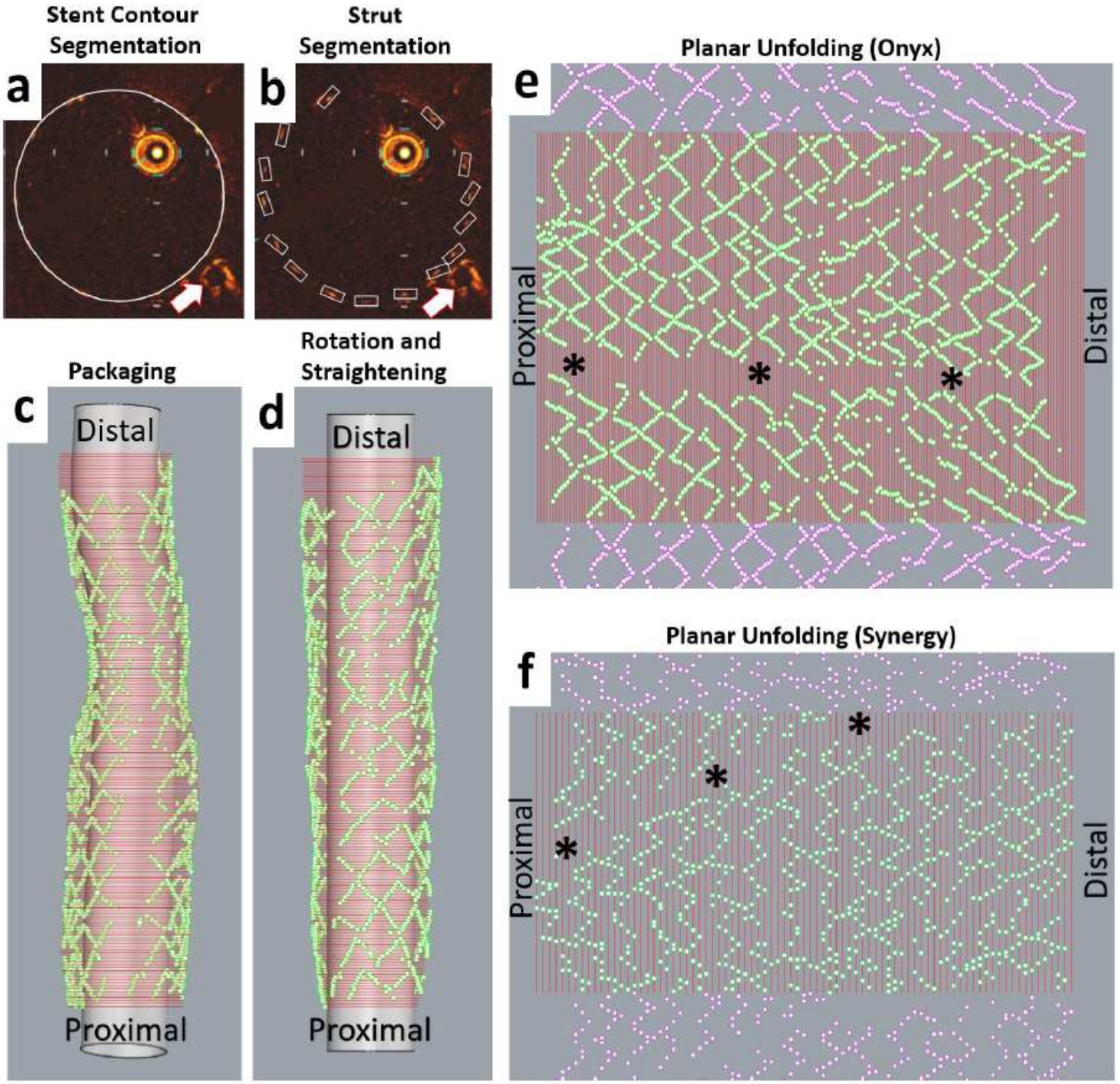

Figure 2

OCT stent segmentation and planar unrolling. (a) Segmented stent contour (white circle) and (b) strut points (white boxes), and arrows indicate the marker, (c) Packaging of segmented stent contours and strut points in space, (d) Rotation and straightening of the packaged stent contours and strut points, (e) and (f) Planar unfolding (stent contours in red, stent strut points in green). The purple strut points were added to show the continuity of stent structure. In (e) and (f) note the zone of missing strut points corresponding to the wire artifact. (a-e) correspond to Onyx stent and (f) to Synergy stent.

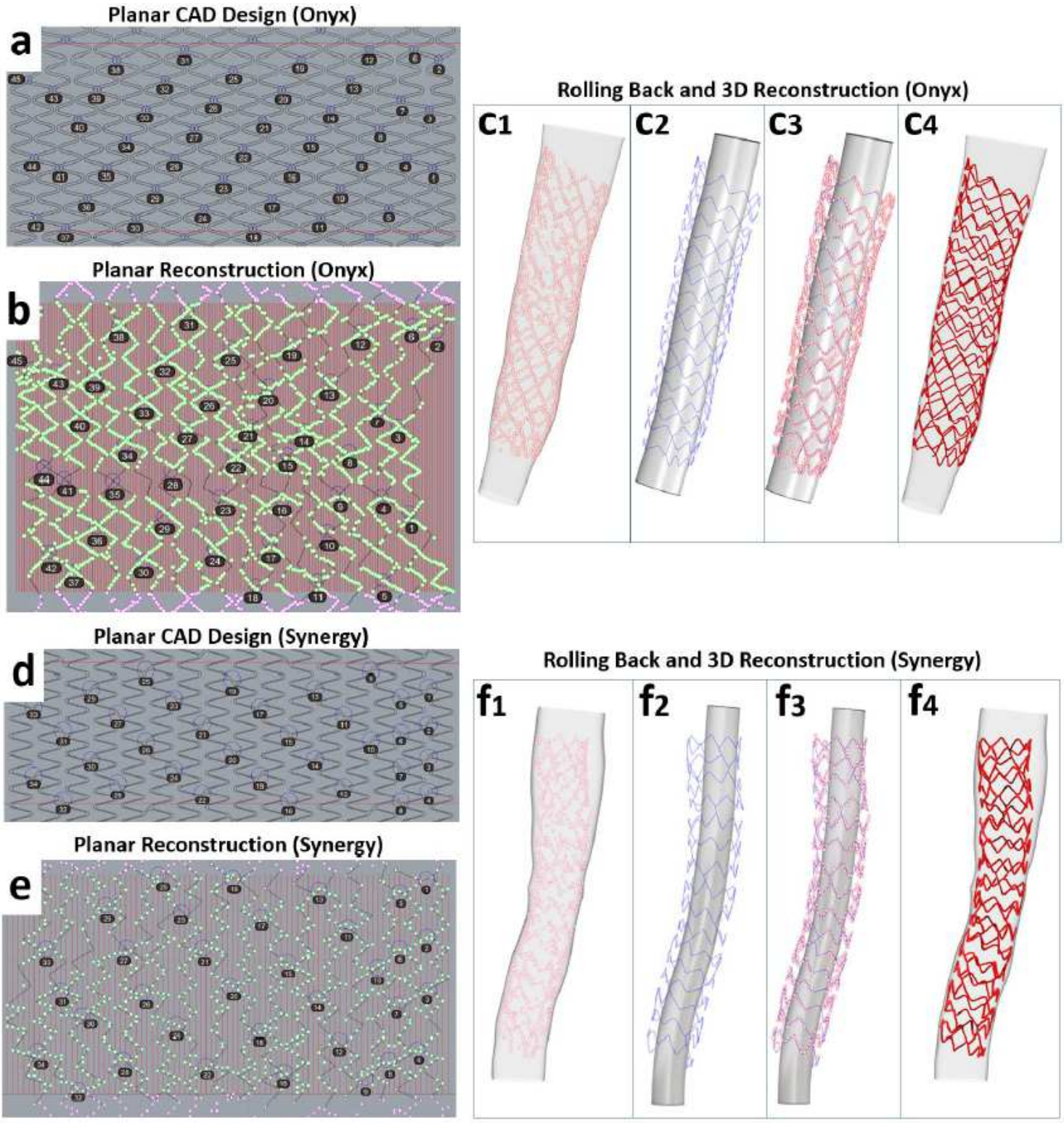

Figure 3

Planar stent wireframe reconstruction and rolling back to space. Planar computer-aided design of (a) Onyx stent and (d) Synergy stent with the boundaries delineated by red lines. Planar stent reconstruction (black lines) of (b) Onyx and (e) Synergy using the unrolled stent strut points and computer-aided stent designs as reference. The numbers and circles in (b) and (e) indicate the location of stent links. Note the extension of black lines beyond the stent boundaries, to show the stent continuity for the next steps.

Rolling back of 2D reconstructed (c) Onyx stent wireframe and (f) Synergy stent wireframe and volume creation: (c1 and f1) 3D reconstructed lumen used as backbone for the 3D stent reconstruction. The red points are segmented stent strut points, (c2 and f2) 3D rolling-back of 2D reconstructed stent wireframe (blue) following the lumen shape, (c3 and f3) Original strut points (red) overlapped on the rolled back stent wireframe, (c4 and f4) Final stent volume generated from stent wireframe. In (c2, c3, f2 and f3) a tube was added inside the stent wireframe for better visualization. Stent designs were kindly provided by the stent manufacturers.

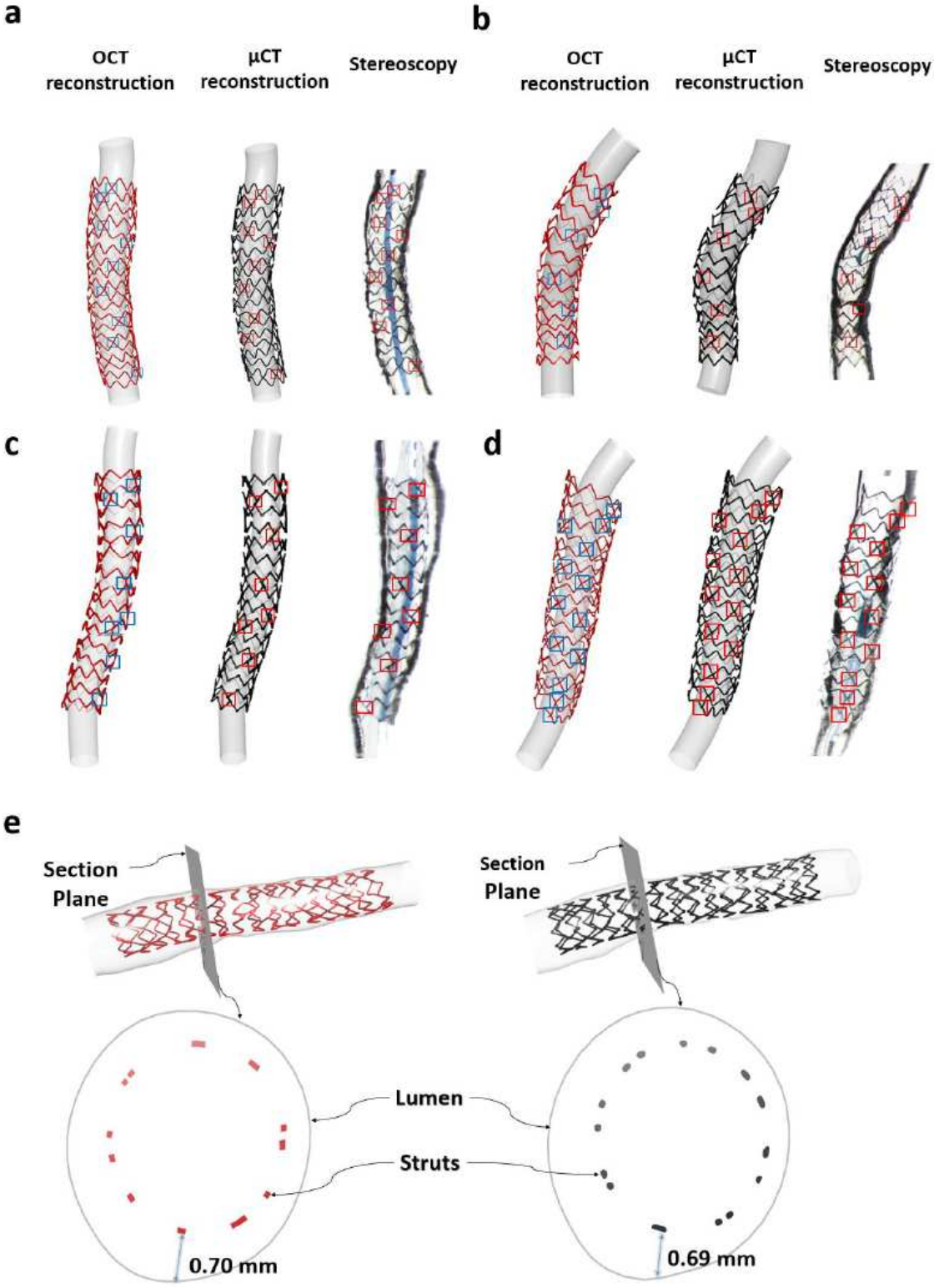

Figure 4

Qualitative experimental validation of stent reconstruction method against μCT and stereoscopic imaging. (a-d) Note the agreement in the link position (blue boxes in OCT-stent reconstructions and red boxes in μCT-reconstruction and stereoscopy). In OCT and μCT-based reconstructed models, a tube was inserted for better visualization, whereas in stereoscopy images a small balloon was inflated in very low pressures for better visualization, (e) Malapposed struts in OCT stent reconstruction at the same location and magnitude compared to μCT.

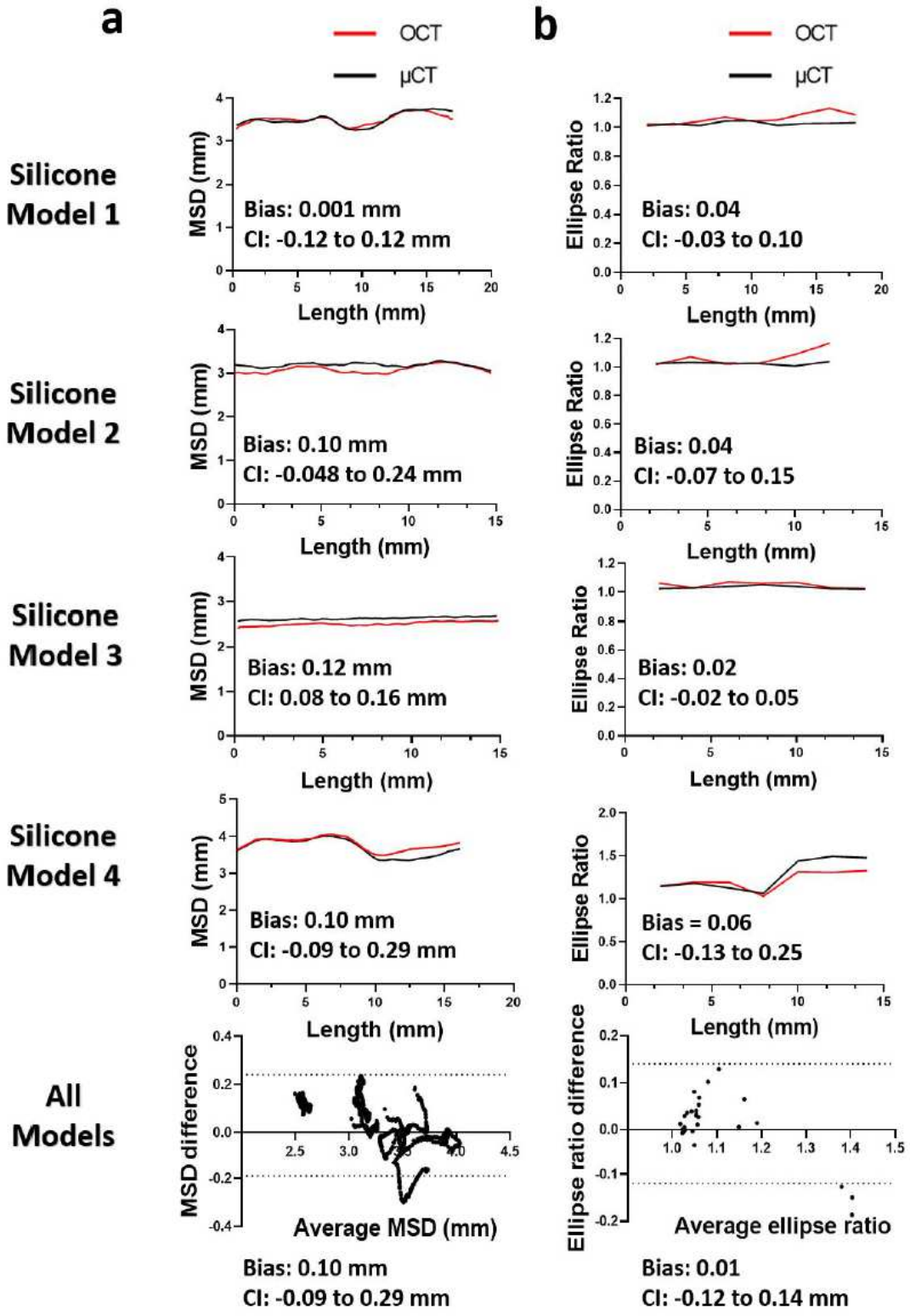

Figure 5

Quantitative experimental validation of stent reconstruction method against μCT. (a) Stent size measured by mean stent diameter (MSD), (b) Stent shape measured by ellipse ratio

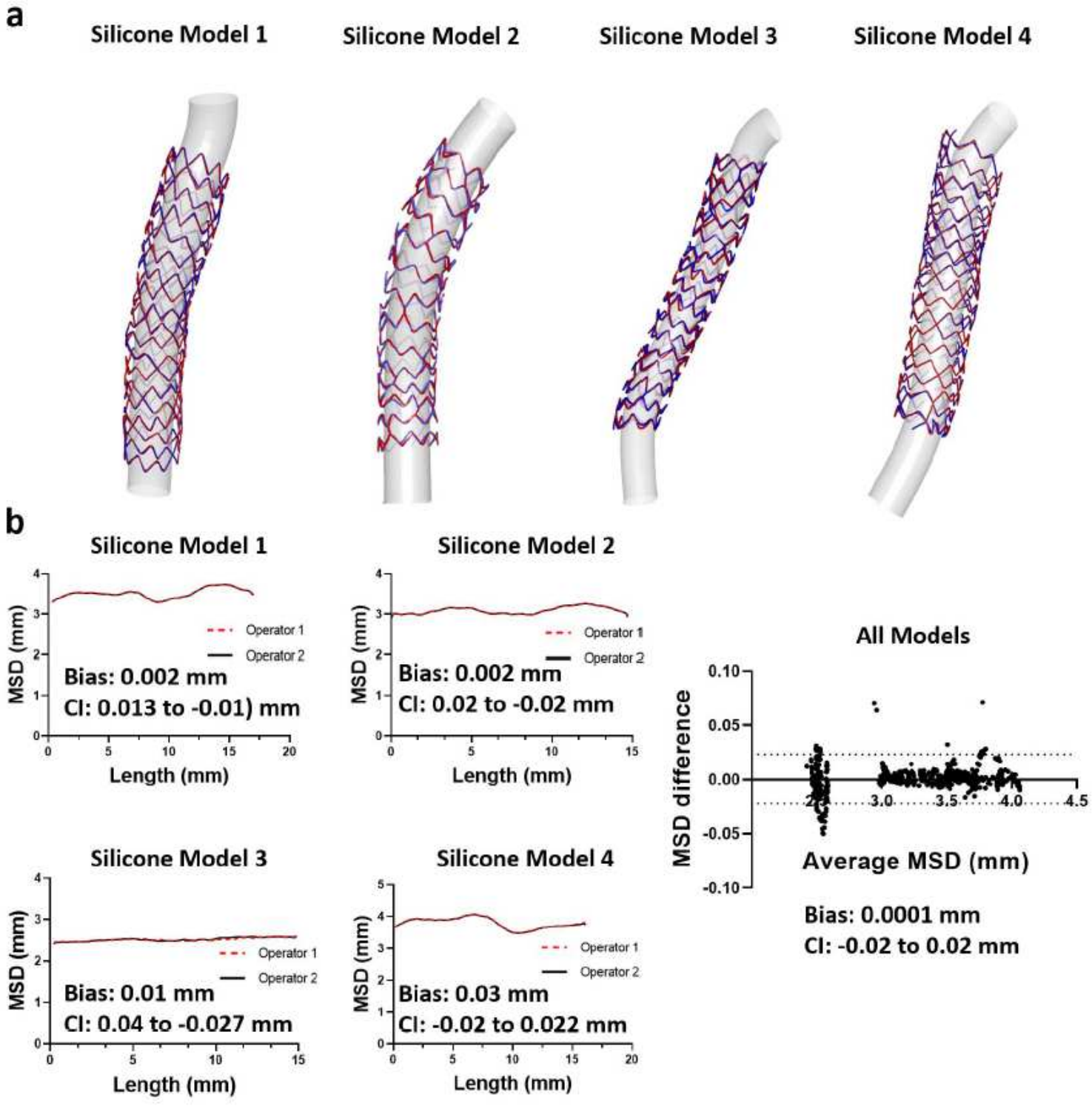

Figure 6

Inter-observer reproducibility of OCT-based stent reconstructions. (a) Qualitative agreement by overlapping the two reconstructed stents. (b) Quantitative agreement for each model (MSD, mean stent

diameter) and overall agreement using Bland Altman analysis

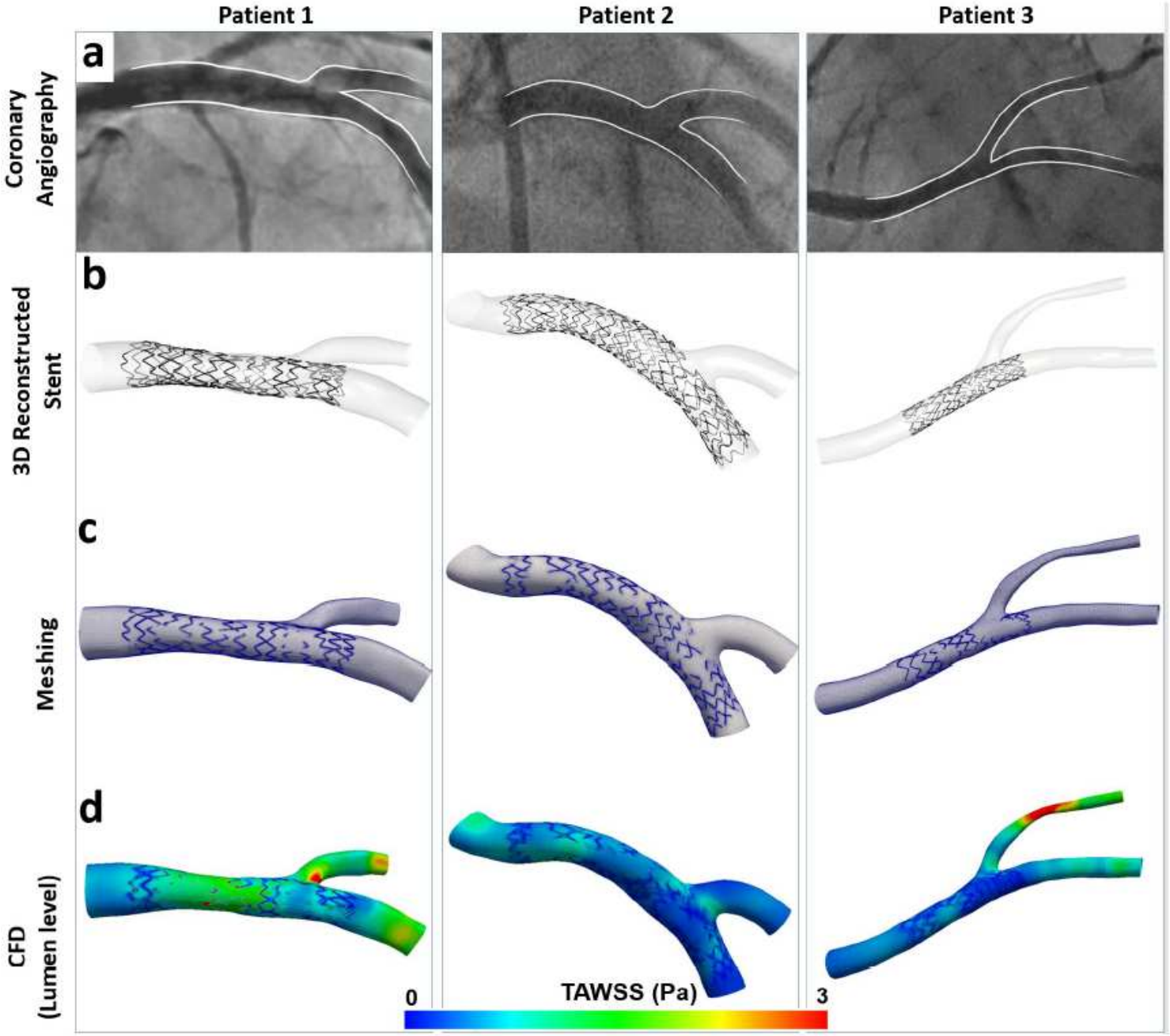

Figure 7

Clinical feasibility of the proposed 3D stent reconstruction method. (a) Invasive coronary angiography post stenting, (b) 3D lumen and stent reconstruction. Note the qualitative agreement to angiography, (c) Lumen and stent meshing, (d) CFD analysis depicting the time-averaged wall shear stress (TAWSS, Pa) along the stented bifurcations.

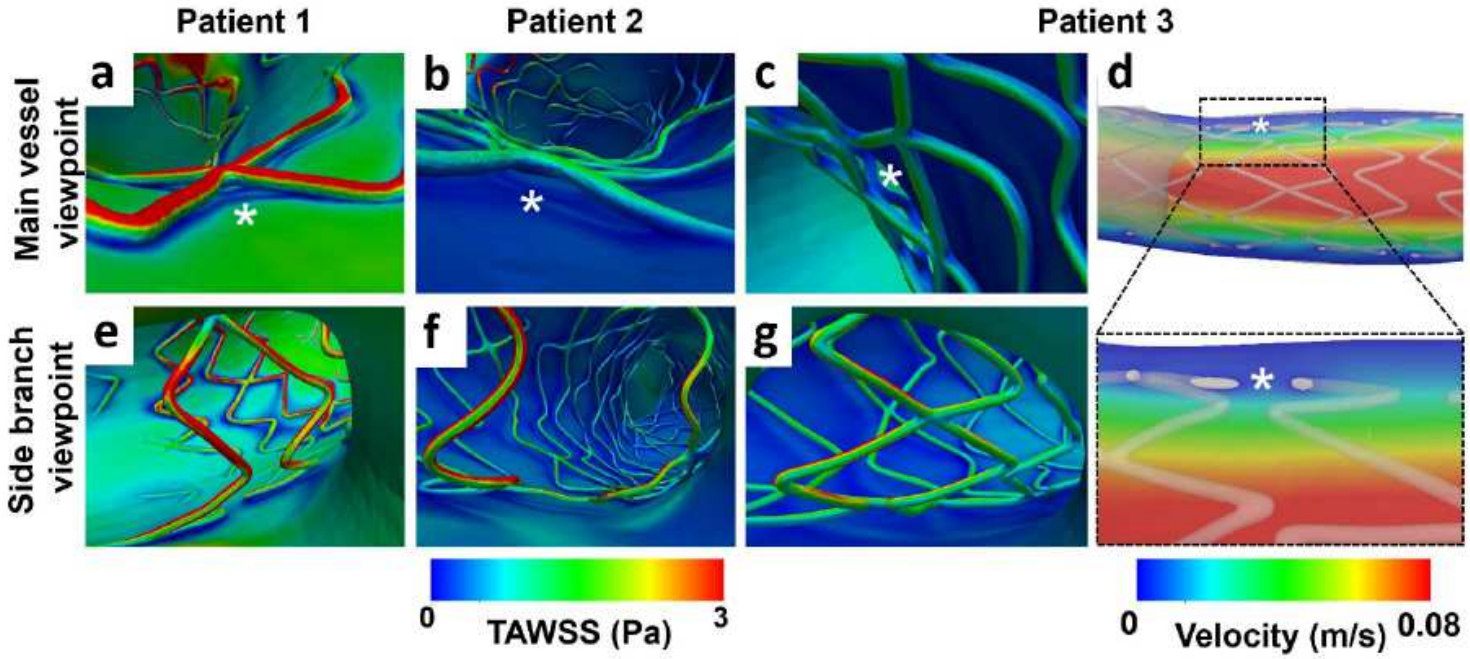

Figure 8

Examples of the calculated hemodynamic micro-environment (strut level) in patient-specific 3D reconstructed stented bifurcations (provisional stenting). (a-c) TAWSS around stent struts. In (a) note the increased shear stress on the luminal surface of a well-apposed strut, and in (b-c) the shear stress distribution around malapoposed struts denoted with white asterisks. In (d) longitudinal section showing the low velocity between the lumen and malapposed struts (white asterisks). (e-g) TAWSS distribution at the ostium of the side branch. Note the struts jailing the ostium of the side branch.

Supplementary Files

This is a list of supplementary files associated with this preprint. Click to download.

- 3DReconstructionofStentSupplementary.docx